Minischool on Few-Body Physics, São Paolo, Brazil, October 6-10, 2014

A.S. Jensen
Department of Physics and Astronomy, Aarhus University, DK-8000 Aarhus C, Denmark
(Dated: September 16, 2014)

Physics understanding begins with realizing which degrees-of-freedom are decisive for the phenomena of interest. With this clarification the simplest few-body systems are discussed in general. The concept of Universality is introduced and illustrated by practical physics examples. The scaling properties of dimensionless radius-energy relations are discussed for two and three-body systems. The qualitative difference for N-body systems with $4 \leq N$ is then described and demonstrated. Different universal structures emerge at various thresholds for binding. This gives rise to halos, borromean and brunnian systems, and the Efimov effect. In general this leads to definition of the broad and very active field of physics, called Efimov Physics.

Coordinate space formalism is sketched by use of the hyperspherical formulation for three-body systems, and illustartive examples are shown. Specific few-body astrophysics processes are discussed in some details.

I. DEGREES OF FREEDOM

Nuclear physics is a subfield of physics which in turn is a science discipline. Nuclear physics is usually understood as the structure and reactions of entities consisting of neutrons and protons. A description includes the interactions between the basic constituents. The field is often extended to include hadron physics, that is the structure and reactions of strongly interacting particles, preferentially neutrons, protons, π, ρ, and ω-mesons.

The fundamental question in scientific descriptions of any specific system is the choice of degrees of freedom. For example (1) stars are the ingredients of galaxies, (2) solar systems are made of sun, planets, moons and dust, (3) the earth is made of water, solid and interior hot core, (4) animals are made of tissues, bones and fluids, (5) plants are made of fibers, (6) bones, tissues, fibers, etc are made of celles, (7) celles are made of bio-molecules, (8) molecules are made of atoms, (9) atoms are made of electrons and the nucleus, (10) the nucleus is made of neutrons and protons and perhaps occasional pions, (11) hadrons are made of quarks, (12) stop so far.

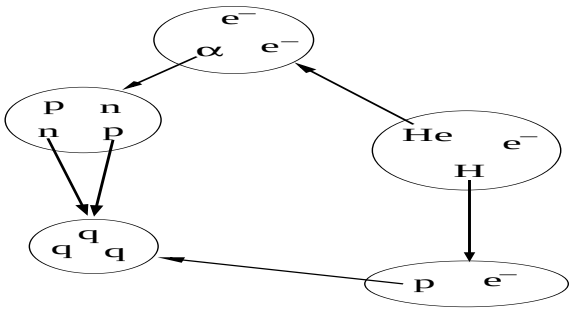

FIG. 1. The hierarchy of degrees of freedom illustrated by the three-body system He + H + e^- (He and H-atoms and an electron) and subdivisions first into an α-particle and nucleons and eventually into quarks.

This list is deliberately far from being exhaustive for several reasons. First many other groups could be mentioned. Second many distinctions and subdivisons could be made. Third mixing and interaction could in addition be made, astro-physics, geo-physics, bio-phyiscs, etc. Relevant for nuclear physics is the families of leptons with electrons, muons, tau-particles and corresponding neutrionos. The connection is that neutrons spontaneously decay into protons, elections, and anti-neutrinos. Within nuclei also protons can decay into neutrons, positrons, and neutrinos. These processes carry detailed and accurate information without affecting nuclear structures. In Fig.1 we illustrate with a proton, an electron, an α-particle (the nucleus of two neutrons and two protons in the He-atom).

This elaborate introduction should make it abundantly clear that practical investigations of specified systems first must choose the ingredients of imminent importance. To study one virus, it is meaningless to start with quarks and leptons, then build nuclei, atoms, molecules, bio-molecules, etc., until the level of a virus is reached. One can to an extremely good approximation assume that the nucleus within the atom is completely inert provided it is stable. Therefore first choose the all-decisive degrees of freedom and understand the systems on this level.

For the structure of nuclei neutrons and protons are the building blocks, and we shall therefore concentraten on combinations of these particles. This is far from excluding analogies with other (preferentially) physics systems. Similarities (and differences) with structures or techniques in other subfields of physics and chemistry are very much present and illuminating. Nuclei are systems of 2 and about 300 particles. This means from detailed few-body $(2, 3, 4, 5)$ to many-body structures, from unavoidable quantum mechanics to classical macroscopic physics, from mean-field average to strongly correlated structures, from individual to collective motion, from very short- to infinte range of the interactions, from strongly bound to weakly or unstable continuum structures with finite lifetime. Thus nuclei are challenging and rewarding to study. Furthemore, they are extremely useful in series of applications, producing energy, dating of small samples, medical use for diagnoses and for treatments, microscopic tracer elements in environmental studies, characterization of materials,

II. FEW-BODY SYSTEMS

The concept of contributing degrees of freedom suggests that an N-body system sometimes can take advantage of arranging its structure in clusters. This can lead to a different hierarchy where relative cluster-cluster degrees of freedom are more important than the intrinsic individual cluster degrees of freedom. The prominent nuclear example is the alpha-particle which is tightly bound with a small radius. It is then suggestive to use it as the building block combined with a few additional neutrons and protons. In general, this structure does not give a very good description for intermediate and heavy nuclei, although reminiscences sometimes can be observed in scattering experiments. The reason can be found by comparing the distance between nucleons within one and between different alpha-particles. As these distances are very similar the alpha-particle cannot exist as an entity in nuclei. However, several light nuclei exhibit alpha-cluster structure combined with additional nucleons.

A. Halo nuclei

We know from the deuteron two-body studies that weak binding and short-range interactions lead to the mean square radius being inversely proportional to the binding energy for s-waves. In general we have

$$\langle r^n \rangle \left(\frac{8\mu B}{\hbar^2} \right)^{n/2} \to n! \, , \tag{1}$$

where μ is the reduce mass and B the binding energy. For a finite angular momentum quantum number, l, the non-normalized nth moment diverges as $(\mu B)^{(2l-n-1)/2}$ for $n \geq 2l-1$ and converges for $n \leq 2l-1$. The divergence is logarithmic when $n = 2l-1$. Thus the probability distribution ($n = 0$) diverges only when $l \geq 1/2$, that is for s-waves. The seond moment (the mean square radius) diverges only when $l \geq 3/2$, that is for s and p-waves.

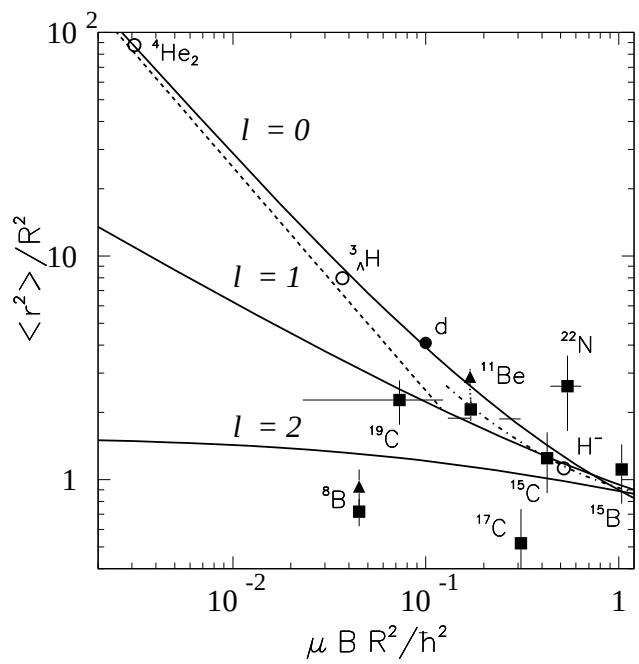

FIG. 2. Scaling plot for two-body halos. The ratio of the halo and the potential square radii as function of the scaled separation energy. The dashed line are pure s-wave Yukawa wave function. The solid and dash-dotted lines are for square-well and r^{-2}-potentials, respectively. The thin horizontal lines indicate where 50% of the wave function is outside the potential. Filled and open symbols are experimental data or theoretical calculations.

The universal character of the two-body radius-energy relation in eq.(1) is illustrated in Fig.2 for the second moment. We also show results for p and d-waves. The divergence and covergence for vanishing binding energy is seen for s, p and d-waves, respectively. We shall return to the realistic systems shown in the figure. They follow roughly the simple scaling rules where deviations can arise from the strong reduction to only two-body degrees of freedom.

We define halos as spatially extended objects measured in terms of the natural length scale of the system, which could be the range of the potential or its effective range. Then two-body halos can only appear in s and p-waves,

provided the binding energy is sufficiently small and the size is measured by the root mean square radius. Higher moments may diverge for vanishing binding energy but then only a smaller fraction, parts of the tail, of the wave function would be located at large distance.

Let us now extend from two to a larger number of clusters, N_c, each of them made of a number of nucleons, in total A nucleons. We perform a transformation from the initial particle coordinates, $\vec{r}_i$, to one overall length coordinate ρ and $d(A-1)-1$ dimensionless angular coordinates. The factor d is from the dimension of space (usually $1, 2, 3$), the subtraction of d is removal of the center of mass degrees of freedom, and subtracting 1 is the coordinate ρ defined by

$$mM\rho^2 \equiv \sum_{i<k} m_i m_k (\vec{r}_i - \vec{r}_k)^2 \ \ , \text{with } M = \sum_i m_i \ , \tag{2}$$

where m is an arbitrary normalization mass. The kinetic energy operator, T, expressed in the new coordinates then becomes

$$T = \frac{\hbar^2}{2m}\left(-\frac{\partial^2}{\partial\rho^2} + \frac{l^*(l^*+1)}{\rho^2} + \frac{1}{\rho^2} D(angles)\right) , \tag{3}$$

where $l^* = (dA - d - 3)/2$ and $D(angles)$ is a function containing first and second derivatives with respect to the angles. Then l^* is a generalized angular momentum which only is conswerved for two particles in spherical potentials. For $d = 3$ and $d = 2$ we get $l^* = 3(A-2)/2$ and $l^* = A - 5/2$, respectively.

If the wave function is isotropic, that is independent of angular directions, then the function D acting on the wave function gives zero. The Schrödinger equation is reduced to contain only the coordinate, ρ, with the effective angular momentum, l^*, and the corresponding centrifugal barrier. We know from two-body structures that spatially extended wave functions only are possible for s and p waves and more mathematically angualr momentum qunatum numbers less than or equal to $3/2$. Thus halos can only appear when $l^* \leq 3/2$ which implies that the particle number $A \leq 3$. Therefore halos of more than three clusters are not allowed for isotropic wave functions.

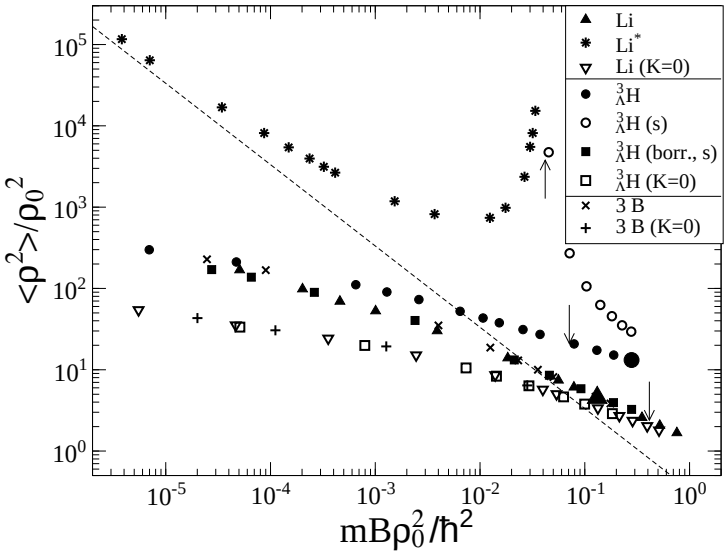

FIG. 3. Scaling plot for three-body halos as in Fig. 2. The dashed line is the Efimov curve for $\nu = 0$. Triangles and stars are for masses corresponding to ^{11}Li (^{9}Li+n+n). Squares and circles are for $^3_\Lambda$H (Λ+n+p). The realistic points are indicated by a large closed triangle and square. Plus signs and crosses refer to three different particles with two fixed scattering lengths while the third is varied. The arrows indicate transitions between Borromean, tango and bound state regions.

The smaller spatial extension of three-body systems is seen in Fig.3. The distinct features are the three curves appearing as the binding energy decreases towards zero. The lowest curve is related to a restricted variational space where no correlations are allowed. The second lowest curve is obtained with all correlations allowed but for a number of different three-body systems and interactions. The highest lying curve emerges in the limit where the Efimov effect appears, that is when the effective potential has the form, $-(\nu^2 + 1/4)/\rho^2$, where ν^2 is a positive number.

The spike in the upper curve at larger binding energy reflects a transition between two- and three-body structures. The three-body structure is on the way to be reduced to a two-body structure where one particle itself has a tightly bound two-body structure compared to the last particle. A survey of possibilities is shown in Fig.4 for three-body systems with different constituents and interactions. We see the regions of unbound, several types of two-body bound,

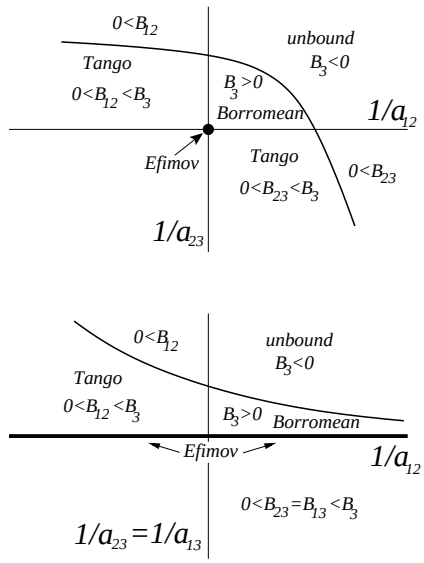

FIG. 4. Regions of stability for three-body systems as function of the inverse s-wave two-body scattering lengths a_{ik}. The point, $a_{ik} = \infty$, is the threshold for two-body binding. The upper part assumes $a_{13} = \infty$, no interaction between particles 1 and 3, and the lower part assumes $a_{13} = a_{23}$.

and three-bound structures. In general three particles become bound for a smaller attraction than that leading to binding of a two-body subsystem.

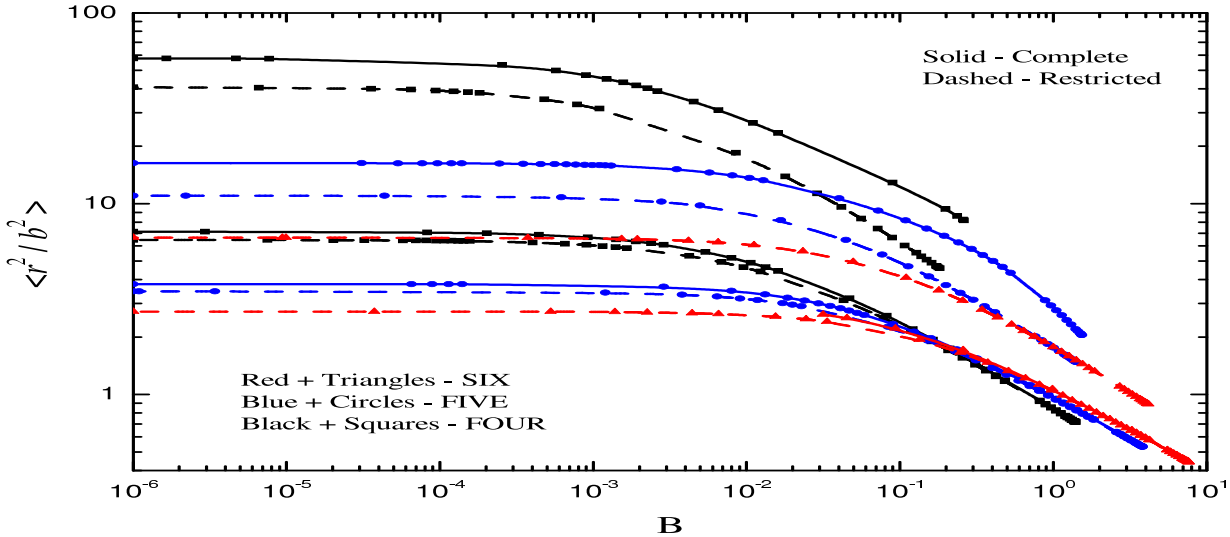

FIG. 5. Mean square radius in units of b^2 as function of the binding energy in corresponding dimensionless units for a gaussian potential of range b for $4, 5, 6$ identical bosons both with complete Hilbert space and for only two-body correlated wavefunctions. Ground state and first excited state are shown for sufficiently large trap length.

Halos of more than three clusters require a different centrifugal barrier, that contributions from the D-operators. This in turn means higher partial waves between some particles or groups of particles, and therefore correlations or equivalently, at least tendencies towards, clusterization. If the correlations become too strong we have effectively reduced the number of clusters. This reduced number of cluster would correspond to a more isotropic wave function, and the argument can be repeated to further reduce the number of clusters. The conclusion is that the fewer clusters the easier it is to obtain large spatial extension. Halos are preferentially made of two or three clusters.

Still more than three particles may form a spatially extended structure provided the attraction is sufficiently weak. For bosons we illustrate this feature in Fig.5 where the four- and five-body bindings are exceedingly small. Unlike the divergences for two and three particles we now find radii converging to a finite value, a constant. This can attributed to the centrifugal barrier for isotropic systems. The remarkable property is that the size at vanishing binding easily can be much larger than the range of the two-body attraction. The average distance between the particles is then

larger the range their mutual interaction. Thay are almost exclusively in regions of zero interaction which therefore only has the role of binding but any detail is unimportant. The structures are universdal or model independent.

B. Universal properties

Halos are not only spatially extended objects, they are examples of structures with universal properties. The meaning of universality is that a large part of the wavefunction can be described without reference to any specific property of the responsible interaction. The structure is model independent which could mean depending only on scattering length where the same value can be reached for completely different potentials.

The first example is then weakly bound two-body structures for short-range potentials. Three particles are from the above discussion seen to have root mean square radii diverging logarithmically with vanishing binding energy. They can then be halos and described as universal structures. When the strength of an attractive pairwise interaction between identical bosons in a three-body system is increased from zero, binding is achieved at some point before the pairs become bound. Thus the three-body system can be bound even when none of the two-body subsystems are bound. Such systems are called Borromean systems, and expected to be universal for sufficiently weak binding energy, see. Figs.4 and 3.

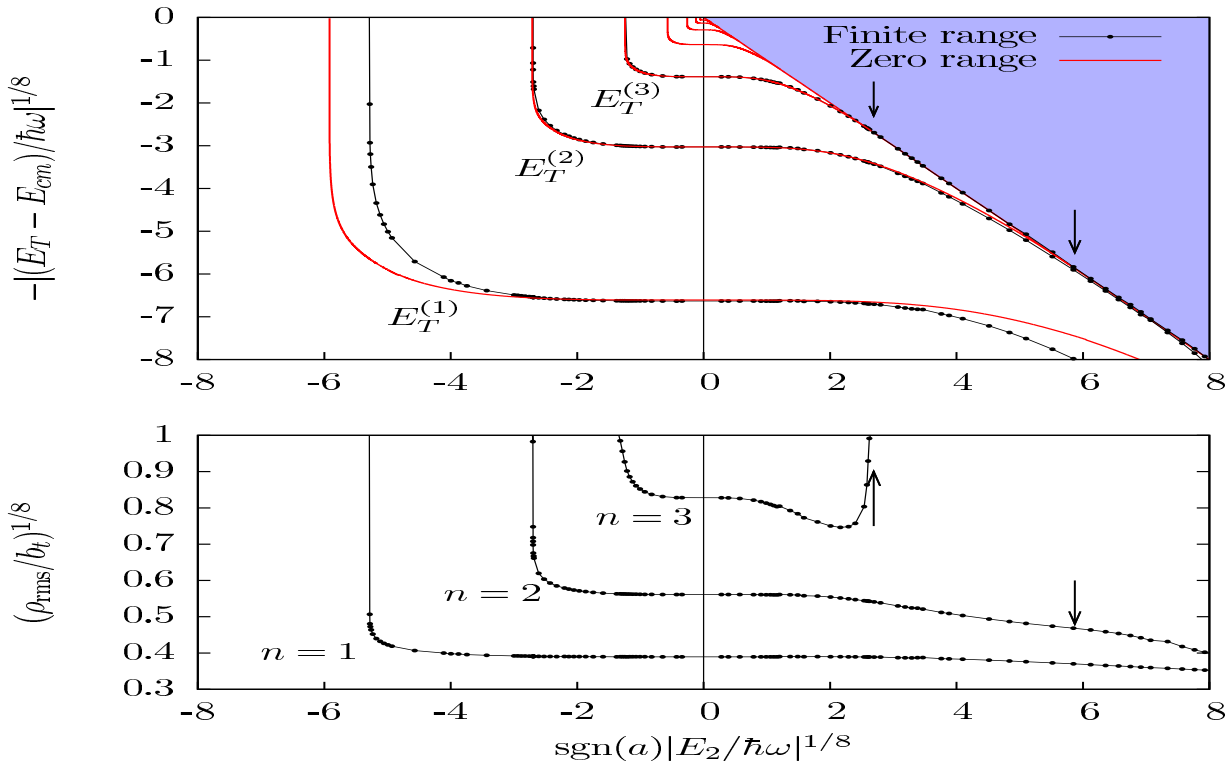

FIG. 6. Three-body energy levels measured as function of the two-body energy. On the right ($a > 0$) is the weakly bound dimer and on the left ($a < 0$) is the virtual dimer energy. The bottom part shows the root-mean square hyper radii. The zero-range predictions (red curves) of the crossing of the Efimov states with the atom-dimer threshold are indicated with arrows.

Another type of universality was discovered as a mathematical anomaly for three bosons when each pair approach binding. Altough the pairs are unbound, the three-body system is already bound, but the number of bound states approach infinity as the pairs approach binding. The radii and binding energies of these infinitely many bound states become exponentially large and small, respectively, that is

$$\frac{B_n}{B_{n+1}} = \frac{< r^2 >_{n+1}}{< r >_n} = \exp(2\pi/\nu) \ , \tag{4}$$

where ν is a real number between 0 and ∞. If existing, these states would be extremely large and qualified for being denoted as giant halos. They are naturally called Efimov states after the physicist who discovered this effect in 1970. These states were searched for in nuclei and molecules for a number of years. Now they are studied in controlled

atomic physics where the effective interaction can be varied over a large range of values, including both sides of pairwise binding and no binding.

The connection between Borromean and Efimov states can be seen in Fig.6 which exhibits the three-body energies as function of the two-body interaction for three idnetical bosons. The cental vertical line distinguishes between unbound (left) and bound (right) two-body systems. Therefore Borromean systems are to the left where the curves show three-body bound state energies. The ground state energy is the lowest curve which approach zero at the point where the attraction is too small to bind even the three-body system. Larger attraction leads to larger binding (lower energy) and more bound state at discrete irregular intervals. Approaching two-body binding increase the number of bound three-body states which becomes infinitely large precisely when the two-body binding energy is zero. This is the Efimov effect which in its clean form occures at that point. All radii and binding energies of these states, except the lowest, are related by the scaling relations in eq.(4).

Stronger attraction produce the two-body binding shown as the decreasing curve separating discrete three-nbody states from the continuum of (bound)dimer-particle states. The peculiar feature is now that the three-body energies decrease slower than the two-body threshold. All energies, except the lowest, therfore merge with the continuum. This simply means that these three-body states have a higher energy than a dimer plus an unbound particle of perhaps zero relative kinetic energy. This implies that the number of bound, stable three-body states decrease from infinity to a finite number.

If a name should be attached to universal structures in physics, it would be natural to choose Vitaly Efimov. Accordingly a new subfield concerned with universality could be named Efimov Physics. The defining keyword is model independence, or universality and scale invariance. Model independence is already described. We can explicitly define "Efimov physics" as the quantum physics where Universality and Scale Invariance apply. By Universality we mean independence of the particular shape of the interparticle potential, or equivalently that the results are describable by use of any interparticle potential where one or a few integral properties are the same. By Scale Invariance we mean independence of the length scale of the system, that is the same description applies on fermi, Ångström , and any other length scale of the system.

These definitions are often confusingly mixed up with the Efimov effect itself, that is by focusing on the Efimov states which differ from each other by a scale factor. The same description applies for each of the states that appear in discrete intervals separated by the scale factor. This is consequently called discrete scale invariance, although the states differ at least by the number of radial nodes. Universality is instead referred to mean that the same theory describes Efimov states at different length scales, and possibly also at different energies in the same system.

The fundamental reason for occurrence of model independent structures is simply that the wavefunction of such a state is located in a classical forbidden region where the potential is negligibly small and the structure consequently determined by the boundary conditions attached to solutions for the free hamiltonian. Then details of the potential are unimportant. For two particles the classical allowed regions are given by the potential being larger than the energy. Already for three particles this definition is ambiguous since the energy can be shared between the particles in uneven, and in quantum mechanics ill-defined, proportions.

C. Halo and cluster nuclei

A number of nuclear examples exist as two-, three-, and perhaps four- and five-body halo states. Also Borromean and the generalization to Brunnian structure can be found in nuclei. The definition of Brunnian systems of N particles is that no subsystem (fewer particles) is bound. Borromean structure is then a subgroup for $N = 3$.

Two-body halos are weakly bound and spatially extended two-body states. Dripline nuclei where the ground state barely is bound then suggest itself. Furthermore, excited states of more stable nuclei for very small separation energies of nucleons or clusters may also form halo states. The tail of the wavefunction is $\exp(-r/r_0)$ where r_0 is related to the binding energy. The extend beyond the nuclear radius is has at least to be larger than about 5 fm corresponding to a binding of less than 1 MeV.

We know already the deuteron which can be said to be both a neutron and a proton halo. The two bound states of ^{11}Be (^{10}Be + n) are pronounced neutron halo states with angular momenta $l = 0, 1$ and separation energies 0.50 MeV and 0.32MeV, respectively. The ground state of ^{8}B (^{7}Be + p) is a proton halo state with $l = 1$ and separation energy 0.138 MeV. A cluster halo state is ^{8}Be (^{4}He + ^{4}He) where the binding energy of 0.092 MeV also is very small. An exotic system is the hypertriton, $^{3}_{\Lambda}$H (^{2}H + Λ), with deuteron surrounded by a Λ-particle which has non-zero strangeness, angular momentum zero and separation energy 0.14 MeV. A number of other two-body halos states are established or suggested, see Fig.2. In all cases the structure is for at least 50% of the probability as a two-body system like the deuteron.

Three-body halos are most efficiently Borromean systems. Otherwise one bound two-body subsystem would easily lead to either too large binding to provide spatial extension or to reduction to an effective two-body system of the

initial three-body structure. The mean square radius increases logarithmically with vanishing separation energy, which implies that the spatial extension easily is more confined than two-body s and p-wave halo states. These three-body halos then seem to be less abundant and less pronounced than two-body halos.

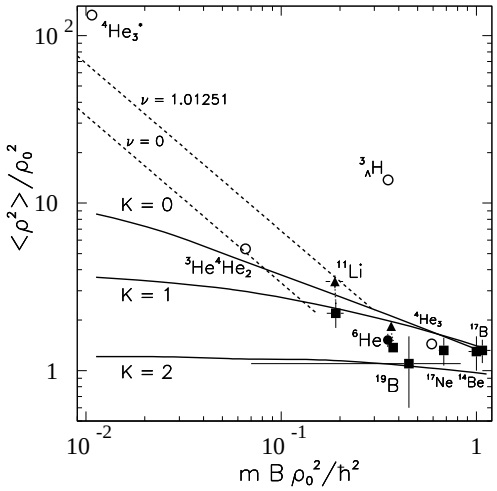

FIG. 7. Scaling plot for three-body halos. The ratio of the halo and effective potential square radii is plotted versus the scaled separation energy. The solid lines are theoretical, scaled curves for different hypermomentum K. The dashed lines show the Efimov states for a symmetric system, $\nu = 1.01251$, and for minimum attraction, $\nu = 0$. Filled symbols are experimental data and open symbols are theoretical calculations.

The three-body halos are more intriguing and the first observation had tremendous impact. The reaction probability is a measure of the size of the colliding systems where the lithium isotopes ($Z = 3$) were combined with an ordinary well described nucleus. The size of ^{11}Li turned out to be much larger than its neighbours and the prediction of the $A^{1/3}$ rule. The explanation is that ^{11}Li (^{9}Li + n +n) is a Borromean system with very small two-neutron separation energy and consequently very large spatial extension. Another well-studied two-neutron Borromean halo system is ^{6}He (^{4}He + n +n). Other suggested Borromean halo systems are ^{20}C (^{18}C + n +n), ^{22}C (^{20}C + n +n), ^{19}B (^{17}B + n +n), ^{9}Be (^{4}He + ^{4}He + n), ^{17}Ne (^{15}O + p + p). We show in Fig.7 a number of these systems in the dimensionless scaling plot of radius versus energy.

Some of the effective two-body halos like ^{8}B and the hypertriton can also be viewed as three-body halos, that is ^{8}B(^{3}He +^{4}He +p) and $^3_\Lambda$H (p + n + Λ). This again reflects the importance of choice of degrees of freedom as for ^{8}He (^{6}He + n + n) and ^{14}Be (^{12}Be + n + n), which also could be viewed as higher order halo systems, that is ^{8}He (^{4}He + 4n), ^{14}Be (^{10}Be + 4n). Brunnian systems would usually have much smaller spatial extension, as ^{10}Be (^{4}He + ^{4}He + n + n), ^{10}C (^{4}He + ^{4}He + p + p).

For light nuclei the combinations are most obvious for alpha-particles combined with neutrons. We already mentioned ^{8}Be and addition of one more alpha-particle leads to ^{12}C which is rather deeply bound. However, the second excited state is the most prominent cluster example, that is the so-called Hoyle state, ^{12}C (^{4}He + ^{4}He + ^{4}He), consisting of three alpha-particles with a negative binding energy of -0.31 MeV. Its importance can hardly be exaggerated as a key reaction, the triple alpha process, is stepping stone to synthesis of the heavier elements in our universe. Its existence was predicted by Hoyle before measurements as necessary to understand the abundance of elements in the universe.

These examples emphasize that light nuclei have very individual properties. They change character by addition of one or very few extra nucleons. This of course makes them difficult to understand and describe but for the same reason also more fascinating. The implication is unfortunately that each of them only can be treated superficially as in the present survey lecture. Complications increase when excited states can be of halo or cluster structure while the ground state has a completely different structure. Since excited states are crucial to a number of reactions, it is often necessary to study the detailed structure of the states of the spectra of each nucleus.

III. THE THREE-BODY PROBLEM

We have to extend our investigations to three particles. For applications this has to be both to ground, bound excited, as well as continuum states at energies higher than the threshold where all three particles are separated.

A. Formulation

The description has to start with the hamiltonian entering the three-body Schrödinger equation, i.e.

$$H = T + \sum_{i<k} V_{ik}(|\vec{r}_i - \vec{r}_k|) \ , \tag{5}$$

where V_{ik} is the interaction between particles i and k, and T is the relative kinetic energy operator for the three particles. To illustrate the key problems and some of the features we use the adiabatic hyperspherical expansion method. First we define relative coordinates (Jacobi coordinates), i.e.

$$\vec{x}_{ik} = (\vec{r}_i - \vec{r}_k)\sqrt{m_i m_k/(m(m_i+m_k))} \ , \ \ \vec{y}_{ik} = (\vec{r}_j - (\vec{r}_i + \vec{r}_k)/2)\sqrt{m_j(m_i+m_k)/(m(m_i+m_k+m_j))} \ , \tag{6}$$

where the mass factors are chosen such that $\rho^2 = x_{ik}^2 + y_{ik}^2$. The hyperradius, ρ, is defined in eq.(2) and independent of choice of initial particles, i and k. We select the set of hyperspherical coordinates, $\{(\rho,\Omega)\}$, where $\Omega = \{(\alpha,\theta_x,\phi_x,\theta_y,\phi_y)\}$ is a short hand notation for the angular coordinates describing the directions of $\vec{x}_{ik}$ and $\vec{y}_{ik}$, and α_{ik} is defined by $\tan\alpha_{ik} = x_{ik}/y_{ik}$).

The kinetic energy operator in these coordinates is then

$$T = \frac{\hbar^2}{2m}\left(-\frac{\partial^2}{\partial\rho^2} - \frac{5}{\rho}\frac{\partial}{\partial\rho} + \frac{\Lambda^2}{\rho^2}\right) \ , \ \ \Lambda^2 = -\frac{\partial^2}{\partial\alpha_{ik}^2} - 4\cot(2\alpha_{ik})\frac{\partial}{\partial\alpha_{ik}} + \frac{\hat{l}_{xik}^2}{\sin^2\alpha_{ik}} + \frac{\hat{l}_{yik}^2}{\cos^2\alpha_{ik}} \ , \tag{7}$$

where $\hat{l}_{xik}$ and $\hat{l}_{yik}$ are the angular momentum operators related to $\vec{x}_{ik}$ and $\vec{y}_{ik}$.

The procedure is then to solve the Schrödinger equation for fixed ρ. This involves the five angular coordinates, Ω, where each of them are confined to a finite interval, unlike ρ which can be infinitely large. The solution is an eigenvalue, $\lambda_n(\rho)$, and the corresponding wave function, $\Phi_n(\rho,\Omega)$. The total wavefunction Ψ is then expanded in terms of these solutions, i.e.

$$\Psi = \frac{1}{\rho^{5/2}}\sum_n f_n(\rho)\Phi_n(\rho,\Omega) \ , \tag{8}$$

where $\rho^{5/2}$ is the three-body equivalent of r leading to the reduced relative radial wave function $u = rR$ for two particles.

The differential equation for the radial wavefunctions, $f_{n=0}$, is found by inserting Ψ into the Schrödinger equation and using the expression for T from eq.(7), i.e.

$$\left[-\frac{d^2}{d\rho^2} - \frac{\lambda(\rho)+15/4}{\rho^2} + Q(\rho) - \frac{2mE}{\hbar^2}\right] f_0(\rho) = 0 \ , \tag{9}$$

where $\lambda = 2\nu(2\nu+2) = K(K+4)$ is related to ν from eq.(4) and K introduce after eq.(11). In eq.(9) we omitted the terms coupling to other radial wave functions, but maintained the diagonal coupling, Q, i.e.

$$Q(\rho) = \langle\Phi|\frac{\partial^2}{\partial\rho^2}|\Phi\rangle_\Omega \ , \tag{10}$$

where the expectation value only is taken over angular coordinates.

The differential equation in eq.(9) has the form of the Schrödinger equation for one particle in a potential. The potential is first of all given by the angular eigenvalue, $\lambda(\rho)$, and second modified by the Q-term. If the motion in the angular coordinates is much faster than in the ρ-direction, the motion is adiabatic in ρ-space where the angular parts are quickly adjusted to different values of ρ. Inclusion of coupling terms in eq.(9) produce a set of coupled equations but still only for one coordinate, ρ. Enough terms must be included to get the desired accuracy. This is therefore called the hyperspherical adiabatic expansion method.

The angular equation (ρ constant) for short-range interactions has simple limiting solutions for both small and large ρ. In fact the solutions are the same for $\rho = 0$ and for $\rho = \infty$, that is the hyperspherical wave functions:

$$\Phi_n(\rho,\Omega) = \sin^{l_x}(\alpha)\cos^{l_y}(\alpha)P_n^{(l_x+1/2,l_y+1/2)}(\cos(2\alpha))Y_{l_x m_x}(\theta_x,\phi_x)Y_{l_y m_y}(\theta_y,\phi_y) \ , \tag{11}$$

where $P_n^{(a,b)}$ are the Jacobi polynomials, $n \geq 0$, and $K = 2n + l_x + l_y$, where $\lambda = K(K+4)$ in the limits of small and large ρ. It is then clear that the potentials multiplied by ρ^2, determined by λ, vary from the same constant through a curve for intermediate ρ-values, and back to the same constant value depending on K. The lowest is obviously for $K = 0$. A pocket in between means attraction at these distances.

The method can give both ground and excited states. Bound states are defined by a negative energy and a wave function decreasing exponentially with distance, ρ, with a rate, κ, determined by the energy, $E = -\hbar^2\kappa^2/(2m\rho^2)$. When the energy becomes positive, unbound solutions exist for all E, but the non-normalizable wave functions now oscillate from intermediate distances to infinity. For special energies and angular quantum numbers the wave function has values at small distance much larger than the amplitude of the oscillations at large distance. These structures are the resonances which can play a decisive role in reactions.

The solutions in the continuum can be calculated with the same method as bound states. If the boundary condition, instead of the correct oscillatory behavior, is chosen as zero at a large hyperradius, we only get discrete energy solutions. The larger distance of the boundary the closer are the energies. The resulting states can be used as approximations to the true continuum solutions. This is also valid for resonances which reveal themselves through the structure of their wave functions.

B. Numerical illustrations of three-body ingredients

The effective hyperradial potentials illustrate the crucial ingredients of the method. In Fig.8 we show the lowest set of coupled adiabatic hyperradial potentials for the angular momenta of the lowest bound states and resonances for ^{9}Be. The interactions are for $\alpha - \alpha$, and α-neutron. In all cases we see that the lowest potential has an attractive pocket at small distance, whereas most of the higher-lying potentials are purely repulsive for all distances. The deepest potentials is found for $3/2^-$ which also turns out to be the ground state.

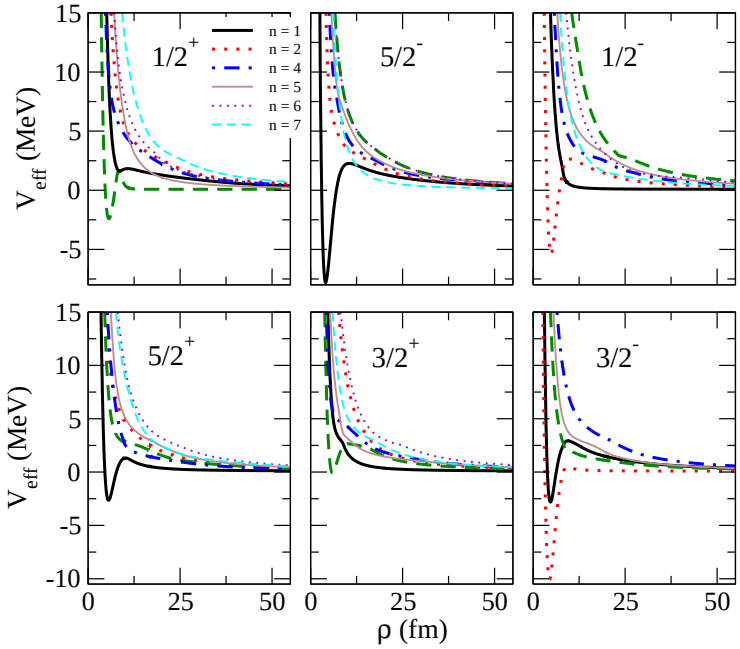

FIG. 8. Real parts of the seven lowest adiabatic potentials as functions of the hyperradius ρ for the $1/2^+$, $5/2^-$, $1/2^-$, $5/2^+$, $3/2^+$ and $3/2^-$ low-lying resonances in ^{9}Be.

Another nucleus which potentially could be of three-body structure is ^{12}C. We show results for the many possible angular momenta in Fig.9. The deepest potential is found for 0^+ which also is the ground state quantum numbers. Furthermore, another 0^+ appear as a very llow-lying resonance, the famous Hoyle state. There is only one excited bound state which has quantum numbers 2^+. It is necessary to emphasize that although we can make three-body computations for any set of (conserved) angular momentum quantum numbers, the resulting states do not have to be even rough approximations of the true physics states. On the contrary, a few states may be well approximated as three-body cluster states, while a number of other states can be absent in three-body calculations. The quantum numbers can still appear for the measured states. This only means that these states must be of completely different structures.

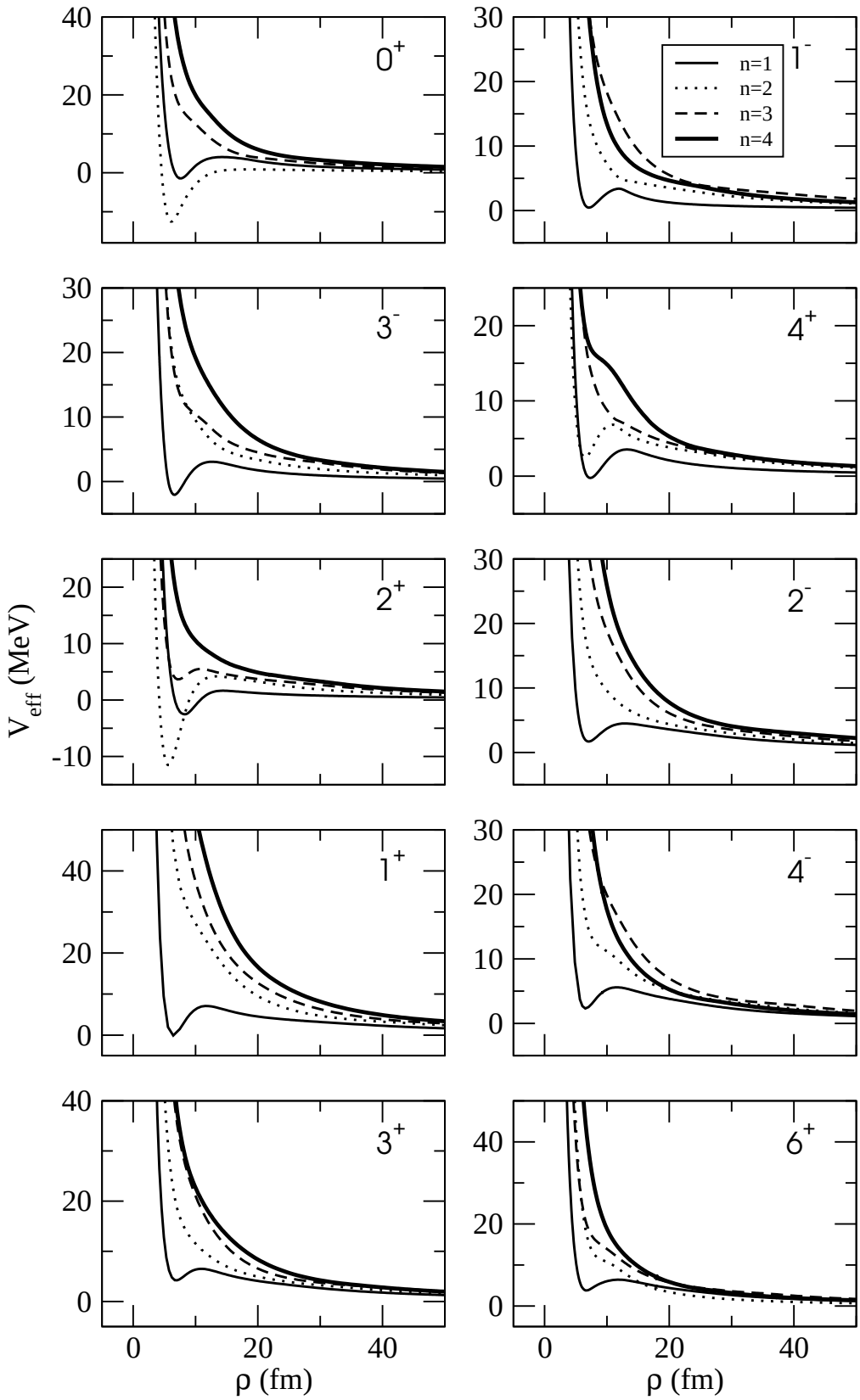

FIG. 9. The real parts of the four lowest adiabatic effective potentials, including the three-body potentials, as functions of ρ for the ^{12}C resonances with J^π given in the figures. The two-body interaction is a slightly modified version of one of the Ali-Bodmer potentials. The parameters (S and b) of the three-body Gaussian potentials, $S\exp(-\rho^2/b^2)$, are adjusted to give the correct energy.

IV. TWO AND THREE-BODY ASTROPHYSICS PROCESSES

In a previous section we superficially mentioned how to proceed from the Big Bang production of Hydrogen (H) and Helium (He) to Carbon (C), and the further on to nuclei of the strongest binding around Iron (Fe). Then the explosions and build up of heavier nuclei through rapid or slow neutron capture, and proton capture along the proton dripline. The delicate pieces of these many processes are for the light systems where the $A = 5, 8$ gaps must be bridged, and at the weighting points at Borromean systems along the proton dripline. We shall consider in some details typical processes where two and three-body reactions are crucial but not fully understood.

Two particles reacting to produce two other (or the same) particles is the simplest non-trivial process to describe. This can already be difficult enough but maybe not sufficiently accurate as only an approximation of the reaction mechanism. In astrophysics complications are that relative energies often are too small to allow experimental tests of model results, and reactions take place through or from continuum states. Furthermore, key processes involve three particles, and it seems unavoidable to employ three-body models instead of the much simpler two-body models. We therefore should use our knowledge of the three-body problem applied to bound states as well as continuum states.

Still, until very recently only results from reduction to two-body problems were available. In most cases they are probably rather accurate in the context. However, such two-body based results are bound to be catastrophically wrong when the total energy is between two and three-body thresholds where the three-body but not the two-body process can proceed. The description may also be very inaccurate when three-body resonances are present or in general when the three-body structure in the continuum contributes beyond two-body approximations.

Three-body methods should by definition be able to provide reaction rates without assumptions about the underlying mechanism. This allows in prinicple the direct reaction mechanism without other specification than initial and final states. This is in contrast to traditional formulations where a two-step process is assumed, that is one two-body reaction into an intermediate structure which reacts with the third particle in another two-body process. This so-called sequential mechanism can be very accurate for example when the intermediate structure is long-lived. To illustrate the content of these models we shall assume simplified descriptions allowing numerical comparison where we first focus on very low temperature.

A. Direct radiative three-body rates

This is from: [7]: Eur. J. Phys. **A47** (2011) 102

The direct three-body radiative capture process, $a + b + c \to A + \gamma$, is related to the reverse photodissiciation reaction, $A + \gamma \to a + b + c$, where a, b and c label the three particles. The reaction rate, $R_{abc}(E)$, for a given three-body energy E is obtained through detailed balance somwhat in analogy to page 264, (but given in Diego et al appendix B, [8]: Eur.Phys.J **A 50** (2014) 93), that is

$$R_{abc}(E) = \nu! \, \frac{\hbar^3}{c^2} \frac{8\pi}{(\mu_{ab}\mu_{ab,c})^{3/2}} \frac{2g_A}{g_a g_b g_c} \left(\frac{E_\gamma}{E}\right)^2 \sigma_\gamma(E_\gamma) \tag{12}$$

where E_γ is the photon energy, $E = E_\gamma + B$ is the initial three-body kinetic energy, B (< 0) is the three-body energy of the nucleus A, μ_{ab} and $\mu_{ab,c}$ are the reduced masses of the a-b two-body system (related to the Jacobi coordinate $\boldsymbol{x}$) and the ab-c system (related to the Jacobi coordinate $\boldsymbol{y}$), respectively, g_i ($i = a, b, c, A$) is the degeneracy meaning what, angular momentum projection, state degeneracy of particle i, and ν is the number of identical particles in the three-body system.

The photodissociation cross section, $\sigma_\gamma(E_\gamma)$, of the A nucleus is assumed to proceed by populating a (three-body) Breit-Wigner shaped resonance of particles a, b, and c with total angular momentum J and energy E_R. Then

$$\sigma_\gamma(E_\gamma) = \frac{2J+1}{2g_A} \frac{\pi\hbar^2 c^2}{E_\gamma^2} \frac{\Gamma_{abc}(E)\Gamma_\gamma(E)}{(E - E_R)^2 + \Gamma^2(E)/4}, \tag{13}$$

where Γ_γ and $\Gamma_{abc} = \Gamma_R$ are the partial decay widths of the resonance for photon and three particle emission respectively, and $\Gamma = \Gamma_{abc} + \Gamma_\gamma$ is the total width. Notice that g_A is the degeneracy of the bound state of nucleus A into which the resonance decays, whereas J is related to the resonance through which the reaction proceeds.

The energy averaged reaction rate is obtained as a function of the temperature T by using the Maxwell-Boltzmann distribution, MB, as weighting function. For three-particles we have

$$MB(E, T) = \frac{1}{2} \frac{E^2}{(k_B T)^3} \exp\left(-\frac{E}{k_B T}\right), \tag{14}$$

where k_B is the Boltzmann constant. The energy averaged reaction rate becomes:

$$\langle R_{abc}(E)\rangle = \nu!\,\frac{\hbar^3}{c^2}\frac{8\pi}{(\mu_{ab}\mu_{ab,c})^{3/2}}\frac{g_A}{g_a g_b g_c} \times\frac{1}{(k_B T)^3}\int_0^\infty E_\gamma^2\sigma_\gamma(E_\gamma)\exp\left(-\frac{E}{k_B T}\right)dE\ . \tag{15}$$

Therefore, once the photodissociation cross section σ_γ for the process $A+\gamma\to a+b+c$ is known, the rate $\langle R_{abc}(E)\rangle$ can be easily obtained. In partucular, it can be obtained directly from the experimental σ_γ cross section.

The result, Eq.(15), has been derived without any assumption about the reaction mechanism leading to the formation of the nucleus A. It is general and applies in particular to capture without population of an intermediate two-body state. Then the width Γ_{abc} corresponds to the width for direct decay of the three-body resonance into particles a, b, and c. We shall refer to Eq.(15) as the reaction rate in the "direct" or "three-body" picture.

B. Sequential radiative three-body rates

This is from: [7]: Eur. J. Phys. **A47** (2011) 102

The sequential process is when the reaction proceeds through an intermediate two-body structure, for example a two-body resonance at some energy E_r in the a-b system. This is treated in two steps where particle a first captures b to populate the intermediate a-b two-body resonant state. In the second step, the a-b system is able, before decaying, to capture particle c, populate some three-body resonance of the nucleus A, and then decay by photo emission into one of the bound states of A.

The reaction rate is given by the rate for the capture of c by the two-body subsystem a-b, $\langle R_{ab,c}(E'',E')\rangle$, weighted with the rate for formation of a-b (can be seen in Angulo et al. NPA656 (1999) 3):

$$\langle R_{abc}(E'',E')\rangle = \frac{\nu!}{1+\delta_{ab}}\frac{8\pi\hbar}{\mu_{ab}^2}\left(\frac{\mu_{ab}}{2\pi k_B T}\right)^{3/2} \times\int_0^\infty\frac{\sigma_{ab}(E'')}{\Gamma_{ab}(E'')}e^{-E''/k_B T}\langle R_{ab,c}(E'',E')\rangle E''dE'', \tag{16}$$

where the total three-body energy, $E=E'+E''$, is given in terms of the relative energy, E'', between particles a and b and the energy, E', of particle c relative to the center of mass of a-b, and σ_{ab} is the a-b elastic cross section. Since δ_{ab} is 1 if a and b are identical particles, and 0 otherwise, we get

$$\langle R_{ab,c}(E'',E')\rangle = \frac{8\pi}{\mu_{ab,c}^2}\left(\frac{\mu_{ab,c}}{2\pi k_B T}\right)^{3/2} \times\int_0^\infty\sigma_{ab,c}(E'',E')e^{-E'/k_B T}E'dE', \tag{17}$$

where the cross section $\sigma_{ab,c}(E'',E')$ for the capture of particle c by the two-body subsystem a-b is related to the photodissociation cross section through the detailed-balance theorem for the two-body system (ab and c), that is

$$\sigma_{ab,c}(E') = \frac{g_A}{g_{ab}g_c}\frac{1}{\mu_{ab,c}\,c^2}\frac{E_\gamma^2}{E'}\sigma_\gamma(E_\gamma)\ , \tag{18}$$

where g_{ab} is the degeneracy of the two-body resonance in the two-body subsystem a-b, and $E_\gamma = E+|B|$, $E=E'+E''$, and E'' is kept constant.

Similarly to the direct process Eq.(13), the photodissociation cross section σ_γ again takes the form:

$$\sigma_\gamma(E_\gamma) = \frac{2J+1}{2g_A}\frac{\pi\hbar^2c^2}{E_\gamma^2}\frac{\Gamma_{ab,c}(E')\Gamma_\gamma(E'+E'')}{(E-E_R)^2+\Gamma(E',E'')^2/4}. \tag{19}$$

This expression is formally identical to Eq.(13), but now $\Gamma_{ab,c}$ refers explicitly to the partial width for decay of the three-body resonance with angular momentum J into the two-body resonance a-b plus particle c. The assumption is that no other decay mode exists, and the direct decay circumventing this two-body path is not allowed, or at least negligibly small. As before, Γ_γ is then the partial width for gamma decay, and $\Gamma=\Gamma_{ab,c}+\Gamma_\gamma$ is the total width.

Replacement of Eq.(18) into (17), and of Eq.(17) into (16) then give the expression for the energy averaged reaction rate:

$$\langle R_{abc}(E'',E')\rangle = \frac{\nu!}{1+\delta_{ab}}\frac{g_A}{g_{ab}g_c}\frac{8\hbar}{\pi c^2(k_BT)^3}\frac{1}{\mu_{ab}^{1/2}\mu_{ab,c}^{3/2}}$$
$$\times\int_0^\infty E''\frac{\sigma_{ab}(E'')}{\Gamma_{ab}(E'')}dE''\int_{E''}^\infty E_\gamma^2\sigma_\gamma(E_\gamma)e^{-E/k_BT}dE \tag{20}$$

where we have replaced the dependence on E' by E by use of $E = E' + E''$. The elastic a-b cross section, σ_{ab}, takes the form, as in Eq.(13) when going through a Breit-Wigner resonance (e.g. Hodgson et al p458):

$$\sigma_{ab}(E'') = (1+\delta_{ab})\frac{g_{ab}}{g_ag_b}\frac{\pi}{\kappa^2}\frac{\Gamma_{ab}(E'')^2}{(E''-E_r)^2+\Gamma_{ab}^2(E'')/4}, \tag{21}$$

where $\kappa^2 = 2\mu_{ab}E''/\hbar^2$, E_r is the energy of the resonance in the a-b system.

The energy dependent widths in Eqs.(13), (19), and (21) are proportional to the penetration factor through the barrier responsible for the correponding resonance ($\Gamma(E) \propto P(E)$). The constant of proportionality is determined by assuming that when evaluated at the resonance energy E_r the width $\Gamma(E_r)$ provides the established (or experimental) width of the resonance Γ_0. This is therefore leading to the expression:

$$\Gamma(E) = \Gamma_0\frac{P(E)}{P(E_{res})}. \tag{22}$$

The expression in Eq.(20) is called the sequential reaction rate.

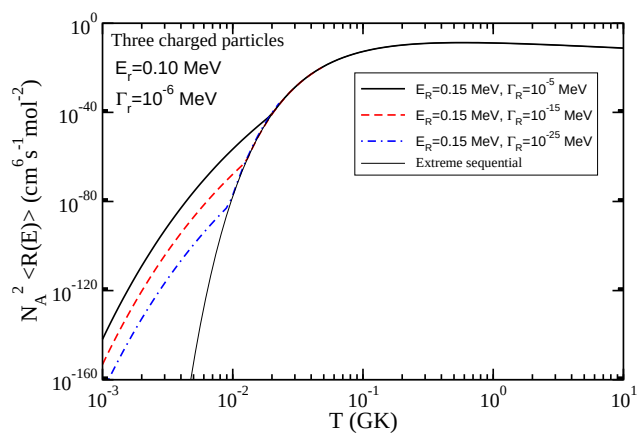

FIG. 10. (color online) Reaction rates in the sequential picture for a system of masses and charges corresponding to three α-particles, but for different small values for the width of the three-body resonance Γ_R. The thick-solid and thin-solid curves are the direct and sequential rates. The dashed and dot-dashed curves are direct rates with $\Gamma_R = 10^{-15}$ MeV and $\Gamma_R = 10^{-25}$ MeV, respectively.

C. Comparing direct and sequential rates

This is from: [7]: Eur. J. Phys. **A47** (2011) 102

We compare in Fig.10 the different approximation for specific sets of parameters. For temperatures higher than about 0.03 GK the rates obtained in the sequential picture are not sensitive to the properties of the intermediate two-body resonance, and the computed rate agrees with the one obtained in the direct picture. This is consistent with the fact that when both two and three-body resonances are very narrow the reaction rate can be approximately obtained by assuming very small width, $\Gamma_{ab,c}$ small but still $\Gamma_\gamma << \Gamma_{ab,c}$, in Eq.(19). Then from Eqs.(15) and (19) we get the energy averaged reaction rate:

$$\langle R_{abc}(E)\rangle = \nu!\frac{2J+1}{g_ag_bg_c}\frac{(2\pi)^3\hbar^5}{(k_BT)^3}\frac{\Gamma_\gamma(E_R)}{(\mu_{ab}\mu_{ab,c})^{3/2}}e^{-E_R/k_BT} \tag{23}$$

which is valid when the two-body resonance energy E_r is below the three-body resonance energy E_R. Otherwise, if $E_R < E_r$ the reaction rate is zero in this limit of very small widths. This is the rate in the extreme sequential picture.

The corresponding rate agrees for $T \gtrsim 0.03$ GK with both the direct and the sequential calculations. At low temperatures this is not true anymore, which shows that the finite width of the resonances influence the rates, and the limit of zero width leading to Eq.(23) becomes increasing invalid. The reason is that the effect from the tails of the resonances, where the penetration factors play a role, is completely absent in Eq.(23). This is also easily recognized in Fig.10, where the thick-solid and thin-solid curves are direct and sequential, and the dashed and dot-dashed curves are the calculations with $\Gamma_R = 10^{-15}$ MeV and $\Gamma_R = 10^{-25}$ MeV, respectively. As we can see, the narrower the three-body resonance the lower the temperature at which the full sequential calculation matches the curve in the extreme sequential picture.

D. The ^{9}Be rate

This is from: [7]: Eur. J. Phys. **A47** (2011) 102

We consider in details the specific case of two α-particles and one neutron, that the $\alpha + \alpha + n \rightarrow {}^9\mathrm{Be} + \gamma$ reaction. The properties of the low energy spectrum of ^{9}Be will determine the reaction rate at low temperatures. The presence of the internal two-body subsystem, ^{8}Be with the very narrow 0^+ resonance at 0.092 MeV, suggests a sequential description of the capture process as an appropriate model.

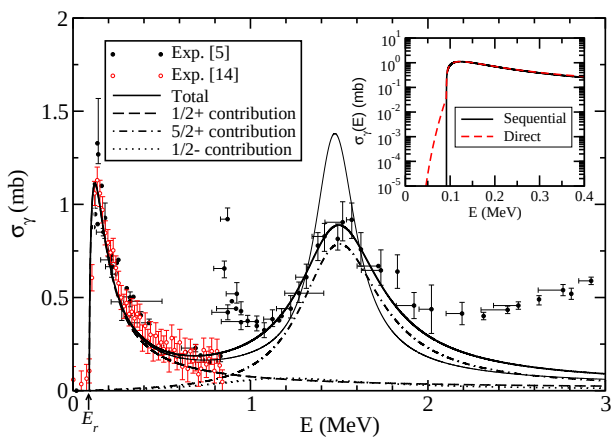

FIG. 11. (color online) Photodissociation cross section for ^{9}Be as a function of the three-body energy E. The solid and open circles are experimental data. The dashed, dot-dashed, and dotted curves correspond to the contribution of the $1/2^+$, $5/2^+$, and $1/2^-$ states in ^{9}Be, respectively. The thick solid line gives the sum of the three contributions. The solid thin line is the total cross section when the $5/2^+$ resonance is parametrized as in NACRE. The vertical arrow in the x-axis indicates the energy of the 0^+ resonance in ^{8}Be. The inner part is a zoom of the low energy region of the cross section, where the solid and dashed lines are the cross section when the sequential and direct pictures are assumed in the low energy region, respectively.

The resulting nucleus, ^{9}Be, has no low-lying and narrow three-body resonance. However, ^{9}Be has a low lying $1/2^+$ resonance in the vicinity of 0.11 MeV, only slightly above the 0.092 MeV of the 0^+ resonance in ^{8}Be. The width of the $1/2^+$ state in a three-body model is estimated to be around 0.1 MeV. In a two-body model this width is estimated to be around 0.2 MeV which makes the resonance extend below the threshold for separation into the three constituents. As a consequence the photodissociation cross section in Fig.11 shows a relatively broad peak at a three-body energy of around 0.11 MeV, in such a way that σ_γ is not negligible in the vicinity of the two-body resonance energy E_r=0.092 MeV.

The experimental data in Fig.11 show that for three-body energies below the 0^+ resonance at 0.092 MeV in ^{8}Be, the cross section essentially vanishes, or at least it is extremely small. This fact supports the assumption that the intermediate 0^+ state in ^{8}Be is actually populated in the process, and therefore the sequential description appears to be appropriate. The energy dependence of the cross section (19) for sequential decay of ^{9}Be into ^{8}Be plus a neutron

is found by use of the energy dependence of the partial widths given in eq.(10.2.25) on page 262, that is

$$\Gamma_{ab,c}(E') = \Gamma_{ab,c}\left(\frac{E'}{E_R - E_r}\right)^{\ell_{ab,c}+1/2} \tag{24}$$

$$\Gamma_{ab}(E'') = \Gamma_{ab}\left(\frac{E''}{E_r}\right)^{\ell_{ab}+1/2}, \tag{25}$$

where $\ell_{ab,c}$ and ℓ_{ab} are the relative orbital angular momenta between particle c and the center of mass of a-b and between particles a and b, respectively, and where the energy dependence of these partial widths are chosen appropriately. Then σ_γ vanishes when $E' = 0$ or equivalently when $E = E_r$. Furthermore, for high temperatures, a pure three-body calculation of the reaction rate, without any additional assumption about the reaction mechanism, agrees reasonably well with the one obtained in the sequential picture.

The behavior of σ_γ at very low energies, also for very small σ_γ, will determine the value of the reaction rate at very low temperatures, and this rate could change depending on which model, direct or sequential, is assumed for the capture mechanism at such low energies. At high temperatures the three-body and sequential pictures provide similar results. For energies higher than E_r we then start by taking the simple parametrization of the cross section used in the sequential description. This gives rise to the cross section shown in Fig.11 by the thin solid line, with an appropriate energy dependence for with $\lambda = 1$, and Eq.(24), has been used for all the resonances. The peak corresponding to the $5/2^+$ resonance is clearly overestimated but properties do not play any role in the low temperature behavior of the reaction rate.

In the inner part of Fig.11 we show a zoom of the low energy region of the photodissociation cross section. When the sequential picture is assumed, the cross section takes the form (19) with $\Gamma_{ab,c}$ given by (24), and then σ_γ vanishes for $E = E_r$, as shown by the solid line in the inset of the figure. However, if for such low energies we assume a direct mechanism, due to the Coulomb repulsion of the two alpha particles, the low energy behavior of the cross section in eq.(13) can be found by the second order WKB transmission rate in eq.(10.2.12). For the Coulomb repulsion the action integral is $b/\sqrt{E}$, that is we get

$$\Gamma_{abc}(E) = \Gamma_{abc}\frac{1 + e^{2b_{abc}/\sqrt{E_R}}}{1 + e^{2b_{abc}/\sqrt{E}}} \tag{26}$$

with

$$b_{abc} = \frac{\pi}{2}\sqrt{\frac{2}{\hbar^2(m_a + m_b + m_c)}}\left(\sum\left(Z_iZ_je^2\right)^{2/3}(m_im_j)^{1/3}\right)^{3/2} \tag{27}$$

where m_a, m_b, and m_c are the masses of the particles and the sum runs over the three possible pairs of particles. The spcific expression for b_{abc} is found by minimizing the path from small to large distance. We use the definition that $\Gamma_{abc} = \Gamma_{abc}(E = E_R)$. The resulting cross section then behaves as shown by the dashed line in the inset of Fig.11.

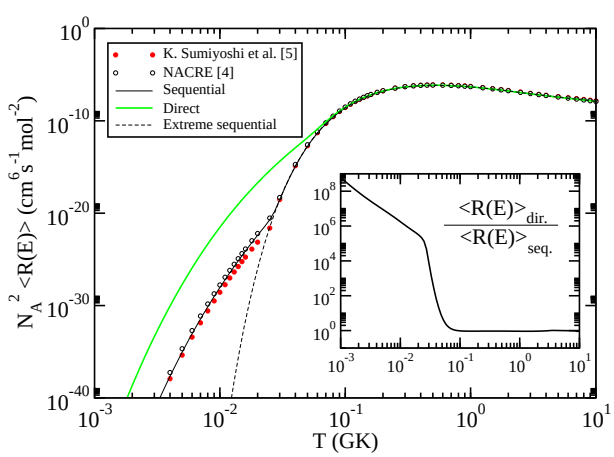

FIG. 12. (color online) Reaction rate for the reaction $\alpha + \alpha + n \to {}^9\mathrm{Be} + \gamma$. The solid points are experimental data and open circles are NACRE results. The dashed line has been obtained in the extreme sequential approximation. The thin solid line is the calculation in the sequential picture (20). The thick solid curve is the calculation (15) assuming a direct capture process at very low energies (dashed curve in the inset of Fig.15). The inset shows the ratio between the thick solid rate (direct capture assumption at low energies) and the thin solid line (sequential capture assumption at low energies).

The reaction rates are shown in Fig.12 for the $\alpha + \alpha + n \to {}^9\mathrm{Be} + \gamma$ process given in a recent experiment, and the NACRE compilation, respectively. They basically agree in the whole temperature range shown in the figure. A correct sequential calculation requires use of Eq.(20), which implies use of the cross section (21) and consequently inclusion of the proper energy tail coming from the decay of the 0^+ resonance in ^{8}Be. When this is done we obtain the rate given by the thin solid line in Fig.12, which, as expected, are below the (almost canonical) NACRE results (open circles) at very low temperatures.

If the low energy tail in σ_γ corresponds to a direct decay mechanism (dashed curve in the inset of Fig.11). In this case, the cross section is given by (13), and the low energy tail takes again the form (26). The reaction rate is then given by Eq.(15), and we obtain the thick solid curve in Fig.12. The reaction rate computed assuming a direct capture at very low energies and the one obtained assuming a sequential capture begin to differ for temperatures smaller than about 0.07 GK. Very soon the rate obtained in the direct picture is several orders of magnitude bigger than the sequential one. This is better appreciated in the inset of the figure, where we show the ratio between both reaction rates. For a temperature of 0.01 GK the reaction rate in the direct picture is almost 7 orders of magnitude bigger than in the sequential picture. The general behaviour of the reaction rates is similar to the one obtained for the triple alpha reaction, although due to the smaller Coulomb repulsion, the absolute values of the rates are now much bigger.

The computed rates are the limiting cases of a fully direct process and a fully sequential process in the very low energy region. If both processes compete, the computed reaction rate would be found in between the thin and thick solid curves in Fig.12. And second, the calculation in the direct picture has been made assuming that $\Gamma_\gamma(E)$ is the same as in the sequential picture, with $\Gamma_\gamma = 0.51$ eV. A change in Γ_γ would imply the same change in the reaction rate.

E. The triple alpha process at low temperature

This is from: [7]: Eur. J. Phys. **A47** (2011) 102

The reaction rate for the triple alpha reaction, $\alpha+\alpha+\alpha \to {}^{12}\mathrm{C}+\gamma$, at very low temperatures is quite controversial. One problem is that now all three subsystems have Coulomb repulsion. In fact, in a recent theoretical work, the reaction rate at a temperature of 10^{-2} GK has been found to be about 20 orders of magnitude bigger than the one given in the (standard) NACRE compilation. Such enormous increase in the reaction rate would have dramatic consequences for the late stages of the stellar evolution in low mass stars. For one reason or another this computation probably gives an incorrect answer.

For very small temperatures the relevant three-body energies in the reaction rate are clearly below the 0.092 MeV of the intermediate 0^+ resonance in ^{8}Be. It is then not so obvious that the sequential picture through that 0^+ state is still appropriate. The occurrence of a direct or a sequential capture mechanism would imply a different behavior of the tail of the photodissintegration cross section (see Eq. (26)), and therefore it would lead to a different reaction rate. This is in fact observed in the schematic case in Fig.10, where an example similar to the triple alpha reaction showed a model dependent rate varying by several orders of magnitude at low temperatures.

In Fig.13 the solid and open circles are the reaction rates for the triple alpha reaction given by Fowler et al. and the NACRE compilation, respectively. The main difference between these rates is found at high temperatures, where the result from Fowler is below the one of NACRE. This is due to the fact that while the effects of the first 2^+ resonance are included in NACRE, they are omitted in Fowler. At low temperatures, both calculations, assuming both a fully sequential capture mechanism, provide essentially the same result. In the calculations shown in this section the lowest 2^+ resonance in ^{12}C has been included using the NACRE resonance parameters.

In the figure, the thin dashed line gives the reaction rate obtained in the extreme sequential model. This approximation amounts to cutting the tail of the cross section for energies smaller than the one of the intermediate 0^+ state in ^{8}Be. This strong approximation gives rise to a reaction rate in good agreement with the results in Fowler and NACRE at high temperatures, while for temperatures smaller than ~ 0.03 GK it clearly underestimates the rate. This is consistent with Fig.10, where we see that a decreasing width of the three-body resonance increases the range of temperatures where the sequential and the extreme sequential calculations agree.

A full sequential description of the process requires the use of Eq.(20). When the Coulomb interaction is decisive, the energy dependence of the partial widths in the sequential picture is changed into:

$$\Gamma_{ab,c}(E') = \Gamma_{ab,c}\frac{1+e^{2b_{ab,c}/\sqrt{E_R-E_r}}}{1+e^{2b_{ab,c}/\sqrt{E'}}} \tag{28}$$

$$\Gamma_{ab}(E'') = \Gamma_{ab}\frac{1+e^{2b_{ab}/\sqrt{E_r}}}{1+e^{2b_{ab}/\sqrt{E''}}}, \tag{29}$$

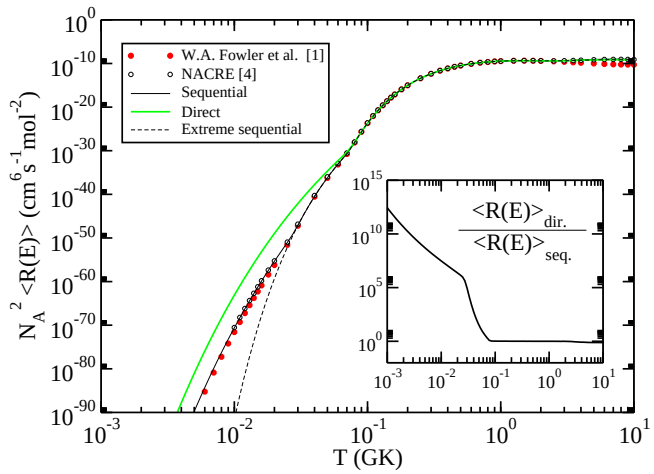

FIG. 13. (color online) Reaction rate for the triple α process. The solid points are from Fowler and open circles are the NACRE results. The thick solid curve is the calculation as in Eq.(15) assuming a direct capture process at very low energies. The thin solid line is the calculation in the sequential picture (20). The dashed line has been obtained in the extreme sequential approximation. The inset shows the ratio between the thick solid rate (direct capture assumption at low energies) and the thin solid line (sequential capture assumption at low energies).

where

$$b_{ab,c} = \frac{\pi}{2}(Z_a + Z_b)Z_c e^2 \sqrt{\frac{2\mu_{ab,c}}{\hbar^2}} \tag{30}$$

$$b_{ab} = \frac{\pi}{2} Z_a Z_b e^2 \sqrt{\frac{2\mu_{ab}}{\hbar^2}}, \tag{31}$$

and where Z_a, Z_b, and Z_c are the charges of particles a, b, and c, respectively, and e is the electron charge.

Compared to the extreme sequential limit, this calculation includes now the low energy tails of the cross sections (19) and (21), which are given by (28) and (29), respectively.

However, when the low energy tail in σ_γ is assumed to be given by (26), which corresponds to a direct capture (dashed curve in Fig.14), and the σ_γ cross section (13) is inserted into Eq.(15), we then get the reaction rate shown by the thick solid line in Fig.13. As we can see, for temperatures smaller than ~ 0.07 GK, the reaction rate obtained assuming a direct capture at very low energies is several orders of magnitude bigger than when the sequential capture is assumed. This is appreciated more quantitatively in the inset of the figure, where we show the ratio between both reaction rates, direct and sequential. We can immediately see that the ratio increases when decreasing the temperature. For a temperature of 10^{-3} GK we have obtained a reaction rate for the direct capture about 12 orders of magnitude bigger than in the sequential picture. This difference reduces to about 7 orders of magnitude for T=0.01 GK.

It is important to note that the computed rates are the ones obtained in the limiting cases of a fully direct or a fully sequential description in the very low energy region. If both processes compete, the computed reaction rate would then be found in between the thin and thick solid curves in Fig.13, which can be taken as the upper and lower limits to the true reaction rate. In any case, even if the process is considered to be fully direct, the increase in the reaction rate compared to the NACRE result at T=0.01 GK is of only 7 orders of magnitude, and thus far smaller then the mentioned 20 orders of magnitude.

We emphasise that the calculations in the direct picture have been made with the same $\Gamma_\gamma = 3.7 \cdot 10^{-3}$ eV in both direct and sequential pictures. A change in Γ_γ implies precisely the same change in the reaction rate, as seen immediately from Eqs.(13) and (15).

F. Triple alpha and resonance structure

This is from [6]: Phys. Lett. **B 695** (2011) 324-328

Surprisingly enough the resonances of ^{12}C are not well known. In fact, the existence of a 2^+ resonance at a relatively low energy is still not experimentally determined. The first of the methods used in this work is the three-body calculation describing radiative capture, see Eq.(12).

The photo dissociation cross section for the inverse process $A + \gamma \to a + b + c$ can be expanded into electric and magnetic multipoles. In particular, the electric multipole contribution of order λ is

$$\sigma_\gamma^{(\lambda)}(E_\gamma) = \frac{(2\pi)^3(\lambda+1)}{\lambda[(2\lambda+1)!!]^2}\left(\frac{E_\gamma}{\hbar c}\right)^{2\lambda-1}\frac{d\mathcal{B}}{dE}\ , \tag{32}$$

where the strength function $\mathcal{B}$ from eq.(10.3.44b) on p284 is

$$\mathcal{B}(E\lambda, n_0J_0 \to nJ) = \sum_{\mu M} |\langle nJM|O_\mu^\lambda|n_0J_0M_0\rangle|^2, \tag{33}$$

where J_0, J and M_0, M are the total angular momenta and their projections of the initial and final states, and all other quantum numbers are collected into n_0 and n. The electric multipole operator is given by:

$$yyyO_\mu^\lambda = \sum_{i=1}^{3} z_i|\boldsymbol{r}_i - \boldsymbol{R}|^\lambda Y_{\lambda,\mu}(\Omega_{y_i})\ , \tag{34}$$

where i runs over the three particles of charges z_i, and where we neglect contributions from intrinsic transitions within each of the three constituents.

Finally the energy averaged reaction rate is obtained as a function of the temperature by using the Maxwell-Boltzmann distribution as weighting function. For three alpha particles, Eq.(15) becomes

$$\begin{aligned}\langle R_{\alpha\alpha\alpha}(E)\rangle = \frac{\hbar^3}{c^2}\frac{48\pi}{(\mu_{\alpha\alpha}\mu_{\alpha^8\mathrm{Be}})^{3/2}}(2J+1)e^{-\frac{B}{k_BT}}\times \\ \times\frac{1}{(k_BT)^3}\int_{|B|}^{\infty} E_\gamma^2\sigma_\gamma^{(\lambda)}(E_\gamma)e^{-\frac{E_\gamma}{k_BT}}dE_\gamma\ .\end{aligned} \tag{35}$$

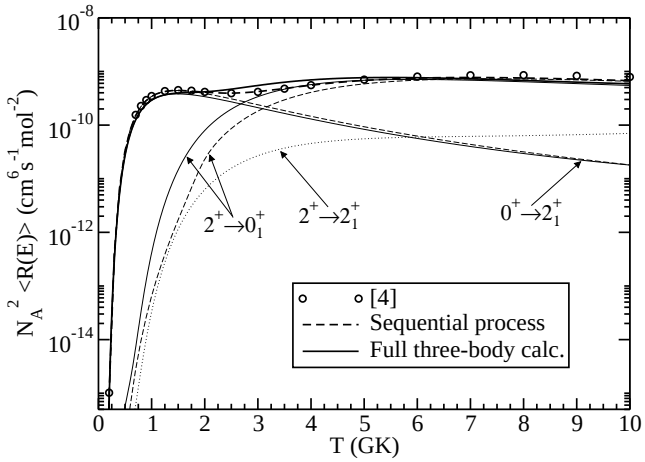

FIG. 14. Reaction rate for the triple α process with the full three-body calculation (thick solid line) and the sequential approach (thick dashed line) as described in the text. The corresponding contributions from the $0^+ \to 2_1^+$ and $2^+ \to 0_1^+$ transitions are given by the thin curves. The dotted line is the contribution from the $2^+ \to 2_1^+$ in the full three-body calculation. The open circles correspond the NACRE rate.

The full three-body method is used to compute the reaction rate for the triple α process. With a specific α-α interaction the ^{12}C spectrum is found, but for all interactions the computed 2^+ resonances appear too often at too low an energy. In particular a 2^+ resonance at 1.38 MeV above the three-body threshold with a width of 0.13 MeV was found in a recent systematic study. The same interaction gives rise to the triple α reaction rate shown by the thick solid line in Fig.14. The contributions coming from the $0^+ \to 2_1^+$ and $2^+ \to 0_1^+$ transitions are shown by the corresponding thin solid lines. The agreement between the total reaction rate and the NACRE result (open circles in the figure) is reasonably good. For completeness, we show in the figure the contribution from the $2^+ \to 2_1^+$ transition (dotted curve). This contribution is very small and could actually be neglected.

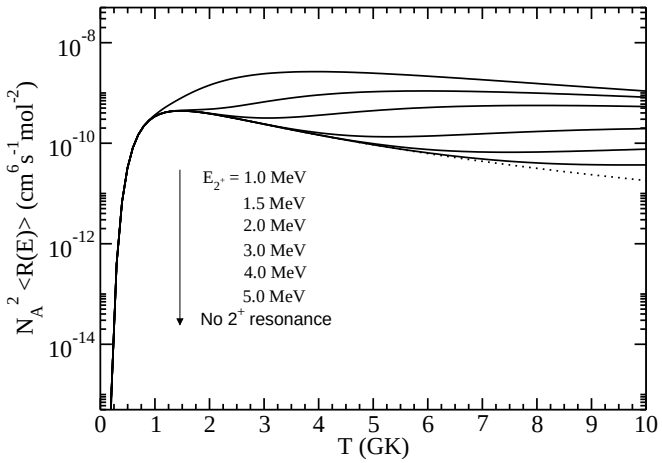

FIG. 15. Reaction rate in the sequential case for different energies of the lowest 2^+ resonance in ^{12}C. The energy increases from the upper curve to the lower from 1 MeV up to 5 MeV. The dotted curve is the calculation where the contribution from the $2^+ \to 0_1^+$ transition has been completely removed.

G. Element production from neutrons and alpha's

This from Europhys. Lett., **90** (2010) 52001.

Elements in the universe heavier than ^{4}He (the α-particle) can essentially be explained as created through step-by-step nuclear reactions in stars. Formation of heavy elements must overcome the problem that all nuclear isotopes with mass numbers 5 and 8 are unstable. When the hydrogen fuel in a star is exhausted, the production of energy by formation of ^{4}He stops and the temperature drops. The subsequent gravitational collapse increases the temperature, and the red giant phase, where helium is now the source of energy, begins. Due to the lack of neutrons in the core of the helium burning red giants, the A=5 and A=8 instability gaps have to be bridged, first of all, by the triple-alpha reaction $\alpha + \alpha + \alpha \to {}^{12}\mathrm{C} + \gamma$.

Other reactions can be conceived for alpha's and nucleons where the charge of the proton decrease the cross sections tremendously at very small energies. In some scenarios also neutrons are present, that is allowing the reactions $\alpha + n + n \to {}^6\mathrm{He} + \gamma$ and $\alpha + \alpha + n \to {}^9\mathrm{Be} + \gamma$. The necessary neutron density can appear at the early Big Bang stages or in the nucleosynthesis related to the type II supernova shock front. In both cases, temperatures are estimated to be of about 7 to 10 GK (GK=10^9 K). With both alpha's and neutrons the $A = 5, 8$ gaps can be overcome through these reactions.

The dominating processes are the electromagnetic radiative recombination of the three particles from continuum to bound state, except at very high densities where four-body recombination can compete favorably. However, the three-body processes producing these nuclei differ from each other. The production of ^{6}He and ^{9}Be is dominated by dipole transitions, while the production of ^{12}C is of quadrupole character.

The production rate P for the capture reaction is obtained after averaging $R_{abc}(E)$ using the Maxwell-Boltzmann distribution as weighting function, and multiplying by the density n_i of particles a, b, and c. This density is usually written as $n_i = \rho N_A X_i / A_i$, where ρ is the density of the environment, N_A is the Avogadros number, A_i is the mass number of particle i, and $X_i = N_i M_i / (N_a M_a + N_b M_b + N_c M_c)$ is the mass abundance of nucleus i expressed by the number of particles N_i and their masses M_i. It is also possible to use the relative abundance defined by $Y_i = N_i / (N_a + N_b + N_c)$.

The three-body recombination can be calculated as described above. The final expression for the production rate P depends then on both, temperature (T) and mass density (ρ) of the environment, which can vary substantially in different scenarios. By rewriting Eq.(15) slightly and multiplying by the densities, we obtain the production rate

$$P_{abc}(\rho, T) = n_a n_b n_c \frac{\hbar^3}{c^2} \frac{8\pi}{(\mu_x \mu_y)^{3/2}} \frac{g_A}{g_a g_b g_c} e^{-\frac{B}{k_B T}} \times \frac{1}{(k_B T)^3} \int_{|B|}^{\infty} E_\gamma^2 \sigma_\gamma(E_\gamma) e^{-\frac{E_\gamma}{k_B T}} dE_\gamma. \tag{36}$$

Density dependence. The density dependence of the production rates in Eq.(36) is very simple for a given temperature. The basic reaction rate for only three particles has to be multiplied by the number of each species of particles. For a given total density ρ found by adding neutron and α-particle densities we can express the density dependence

as $\rho^3 X_\alpha^n X_n^{3-n}$, where $X_n = 1 - X_\alpha$ and X_α are the mass fraction of neutrons and α-particles. Then $n = 1, 2, 3$ correspond to production of ^{6}He, ^{9}Be and ^{12}C, respectively.

When no α-particles are present, $X_\alpha = Y_\alpha = 0$, the production rates are all zero. When only α-particles are present, $X_\alpha = Y_\alpha = 1$, only ^{12}C can be produced. The density dependence for production of ^{6}He and ^{9}Be are each others reflection in $X_\alpha = 1/2$ but pushed towards smaller values as function of Y_α. The production of ^{12}C increases monotonically as function of X_α and Y_α.

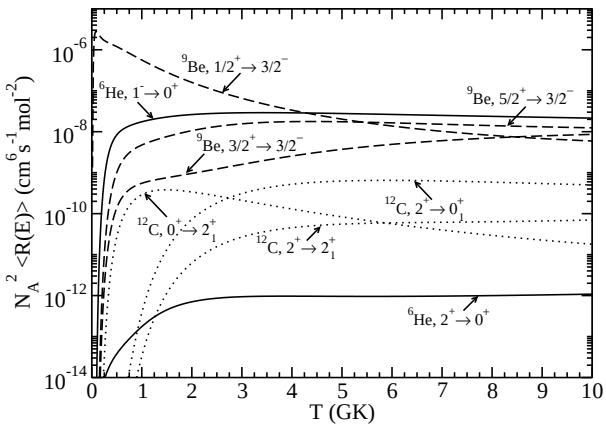

FIG. 16. The rates as functions of temperature for producing ^{6}He, ^{9}Be and ^{12}C in their respective ground states from various continuum states. From 1^- and 2^+ to 0^+ for ^{6}He (solid curves), from $1/2^+$, $3/2^+$, and $5/2^+$ to $3/2^-$ for ^{9}Be (dashed curves), from 2^+ to the 0^+ ground state and from both 0^+ and 2^+ to 2^+ excited bound state for ^{12}C (dotted curves).

The temperature dependence is obtained by folding the calculated energy dependence with the Boltzmann distribution as seen formally in Eq.(36). The different transitions are compared in Fig.16. The production rate for ^{9}Be is by far the largest at low temperatures but matched for ^{6}He above temperatures of $T \approx 4$ GK. The rate for production ^{12}C is much smaller in this temperature range.

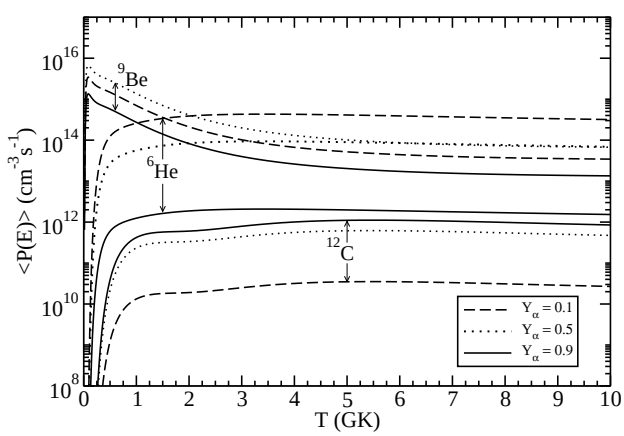

FIG. 17. The numbers of produced ^{6}He, ^{9}Be and ^{12}C per unit time and volume as functions of temperature for Y_α =0.1 (dashed), 0.5 (dotted), and 0.9 (solid) and a density ρ=1 g/cm^3.

The complicated temperature dependence in Fig.16 can now be combined with the simple density dependence, $n_a n_b n_c$, in Eq.(36). After adding up the different contributions for each of the three nuclei we find the creation probabilities shown in Fig.17 as functions of temperature for three different relative fractions of the three nuclei. Creation of ^{12}C only becomes competitive for any temperature when Y_α is close to unity, i.e. when essentially only α-particles are present.

The slightly increasing ^{6}He curves cross the slightly decreasing ^{9}Be curves while the ^{12}C curves stay below for all temperatures below 5 GK. Thus unless the relative α-neutron abundance is extreme we get dominance of ^{9}Be at small temperature and dominance of ^{6}He at large temperature. However, now it is important precisely which number of neutrons and α-particles are available for the recombination process. When $Y_\alpha = 0.1$ the dominance changes from ^{9}Be to ^{6}He at $T \approx 1.5$ GK. For Y_α values larger than 0.5 ^{9}Be dominate for all temperatures.

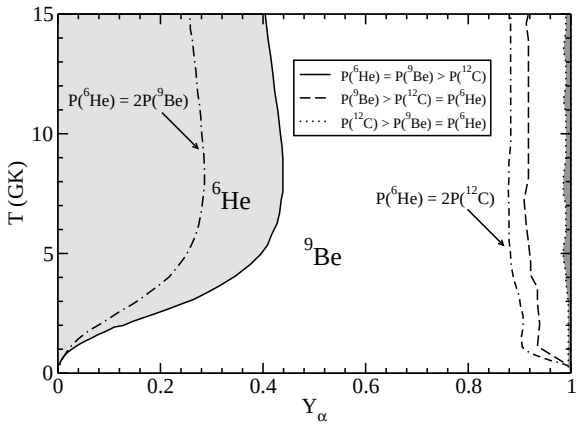

FIG. 18. The phase diagram for producing ^{6}He, ^{9}Be and ^{12}C in the Y_α-temperature parameter space. The curves correspond to a constant ratio of production rates of two nuclei.

The complete picture of the density-temperature dependence of the creation of the three nuclei is shown in Fig.18. For Y_α less than about 0.2 and temperatures above $T \approx 1-4$ GK the nucleus ^{6}He is produced more than twice as often as ^{9}Be. As Y_α increases the relative ^{9}Be production increases and becomes dominant for all temperatures when Y_α exceeds 0.4.

By further increase of Y_α the relative creation rate of ^{12}C increases. At $Y_\alpha \approx 0.88$ the ^{9}Be production is still dominating when ^{12}C is created with half the rate of ^{6}He. At $Y_\alpha \approx 0.92$ the production rates for ^{12}C and ^{6}He are equal, but the production of ^{9}Be still dominates. Only when Y_α is larger than about 0.98, where very few neutrons are present, the production rate of ^{12}C exceeds the other rates. These relative rates are very crudely independent of temperature except for very low Y_α values. Except for the small Y_α results, similar overall conclusions are obtained in most previous investigations.

[1] N.T. Zinner and A.S. Jensen
Comparing and contrasting nuclei and cold atomic gases
J.Phys. **G 40** (2013) 053101.
[2] A.S. Jensen, K. Riisager, D.V. Fedorov and E. Garrido,
Structure and reactions of quantum halos,
Rev. Mod. Phys. **76** (2004) 215-261.
[3] E. Nielsen, D.V. Fedorov, A.S. Jensen and E. Garrido,
The three-body problem with short-range interactions,
Phys. Rep. **347** (2001) 373-459.
[4] A.S. Jensen, E. Garrido and D.V. Fedorov,
Three-Body Systems with Square-Well Potentials in L=0 States, Few-Body Systems, **22**, 193-236 (1997).
[5] R. de Diego, E. Garrido, D.V. Fedorov, A.S. Jensen
Relative production rates of ^{6}He, ^{9}Be, ^{12}C in astrophysical environments
Europhys. Lett., **90** (2010) 52001, pp5.
[6] R. de Diego, E. Garrido, D.V. Fedorov, A.S. Jensen
The triple alpha rate and the 2^+ resonances in ^{12}C
Phys. Lett. **B 695** (2011) 324-328
[7] E.Garrido, R. de Diego, D.V. Fedorov, A.S. Jensen
Direct and sequential radiative three-body reaction rates at low temperatures
Eur. J. Phys. **A 47** (2011), 102-113.
[8] R. de Diego, E.Garrido, D.V. Fedorov, A.S. Jensen
Production of ^{6}He and ^{9}Be by radiative capture and four-body recombination
Eur.Phys.J **A 50** (2014) 93.